Study of the Beach Zone of Koutsounari (SE Crete) using Video Monitoring Methods

A. Kikaki[1], G. Ghionis[1,2 *], M. Vousdoukas[3,4], A. Karditsa[1], O. Andreadis[4], S. Petrakis[1], A. Alexandrakis[2], D. Sifnioti[1], I. Monioudi[4], T. Hasiotis[4], S. Poulos[1], A. Velegrakis[4], N. Kampanis[2], M. Lipakis[5]

1 Department of Geology & Geoenvironment, University of Athens,Panepistimioupolis, Zografou 157 84, Greece, akikakh@hotmail.com, gghionis@geol.uoa.gr, kkarditsa@geol.uoa.gr, spetrakis@geol.uoa.gr, dsifnioti@geol.uoa.gr, poulos@geol.uoa.gr

2 Institute of Applied and Computational Mathematics, FORTH, Nikolaou Plastira 100, Vasilika Vouton, 700 13 Heraklion, Greece, gghionis@otenet.gr, alexandrakis@iacm.forth.gr, kampanis@iacm.forth.gr

3 Joint European Research Center, Institute of Environment and Sustainability, Via Enrico Fermi 2749, I-21027-Ispra, Italy, michalis.vousdoukas@jrc.ec.europa.eu

4 Department of Marine Studies, University of Aegean, University Hill, Mytilini, Greece, vousdoukas@gmail.com, Olympos@aegean.gr, imonioudi@marine.aegean.gr, hasiotis@aegean.gr, afv@aegean.gr

5 Crete Development Organisation, 3 Mahis Kritis Str., Heraklion, Crete, 713 03, Greece, m.lipakis@oakae.gr

** Corresponding author*

Abstract

Coastal zones are among the most active areas on Earth, changing their shape from day to day, or even from hour to hour. The present study investigates the application of video monitoring methods for mapping the beach evolution and the shoreline changes of the microtidal Koutsounari beach in SE Crete. A video-based coastal imaging system consisting of two cameras, installed on the upper beach at an elevation of 14 m above MSL, was used to monitor the study area from 26 November 2012 to 26 May 2013, acquiring images at a rate of 4 Hz for 10 min every hour of daylight. The extraction of the successive shoreline positions was based on 1363 variance images (SIGMA) using specially developed software. Analysis of the recorded shoreline displacements showed that during most of the time the whole length of the shoreline responds in unison (either advancing or retreating) to changes in hydrodynamic conditions. During storms the shoreline retreats, as erosional processes prevail, but recovery is rapid (within 24 h) after the storms. Four shoreline rotation events were recorded, associated with ESE-SSE and SSW incoming waves, which induced increased longshore transport rates. The highest recorded wave run-up was 1.0 m. The eastern part of the beach is more vulnerable to the prevailing wave direction (ESE-SSE) and significant wave heights than the western part.

Keywords

Shoreline evolution, pivoting, video monitoring, beach erosion

1. Introduction

Mapping changes of beach, shoreline and nearshore zone is essential for coastal planning and management. Shorelines migrate due to various factors: human intervention, extreme storms and surges, elevation of the mean water level and swash fluctuations, changes in the shore sediment budget, seasonal changes in storm wave conditions, including wave height, storm duration, alongshore sand supply and the trend of the rising sea level. Nowadays, 28.6% of the total coastline in Greece and 65.8% of the total coastline of Crete are under erosion (EUROSION, 2001). This fact makes the development of new methods for monitoring and mapping the morphodynamic and hydrodynamic changes imperative.

Monitoring of nearshore systems has traditionally relied on in situ measurements of hydrodynamic and morphological changes. These traditional technologies provide data of high quality but with limited spatial resolution and at high costs. The use of aerial photographs to study shoreline variations since 1927 and, more recently remote sensing from satellites have improved the spatial coverage of measurements, but the costs remained high (Crowell et al., 1991). On the other hand, video-based remote sensing offers a good opportunity to monitor the coastal environment at relatively low costs. Video methods allow non-intrusive, continuous measurements at temporal and spatial scales and resolutions for which in situ data collection would demand much greater inputs of personnel, equipment and costs (Vousdoukas et al., 2011).

The use of video for coastal monitoring was introduced by the Coastal Imaging Lab of Oregon University at the beginning of the 1990s. Their system is known as Argus and it is now used all over the world for coastal zone management. With the increasing offer of better and cheaper video cameras and technologies, several systems have been developed in order to evaluate the risks of erosion, the evolution of shoreline, the nearshore bathymetry/topography, the sediment transport and currents, and the stability of coastal structures such as seawalls (Holman and Stanley, 2007).

In Europe, the BEACHMED-e project was launched in 2005 as a result of the collaboration among nine regional partners of four EU nations: Italy, France, Spain and Greece. For the subproject OpTIMAL (Optimisation of Integrated Monitoring Techniques Applied to Coastlines) several video systems were installed along the coastline of Mediterranean Sea in the framework of Integrated Coastal Zone Management. Four different systems were used during this project for coastal video-monitoring: Argus, EVS, KOSTA and Beachkeeper. The main differences among them lie in the type of camera used, while the types of images and products that are produced are similar. The field of view can cover up to 180º, corresponding to a stretch of coast up to 6 km long, depending on the height of the center of view (COV) of the camera and on the focal length of the lens (Archetti et al., 2008).

The use of video cameras for coastal monitoring is documented in scientific literature covering swash processes (Stockdon et al., 2006), wave run-up observations (Vousdoukas et al., 2009), coastal vulnerability assessment based on video wave run-up observations (Vousdoukas et al., 2012), intertidal bathymetry (Aarninkhof et al., 2003), beach cusps (Vousdoukas, 2012) and specialized image processing algorithms applied to identify coastal features of interest such as the horizontal position of the shoreline (Holman and Stanley 2007). Plant and Holman (1997) presented an approach for automatic shoreline extraction, based on the identification of the shoreline intensity maximum (SLIM) position, along cross-shore pixel intensity transects. The pixel intensity clustering (PIC) method is based on hue-saturation-value (HSV) colour pixel intensity differences (Aarninkhof et al., 2003), while artificial neural network (NN) classifiers have also been used (Plant et al., 2007).

2. Study area

The Koutsounari beach is a micro-tidal beach located 8 km west of the city of Ierapetra in the SE part of the island of Crete. The climatological data from the Hellenic Meteorological Service weather station at Ierapetra and the in situ measurements indicate that the nearshore zone at Koutsounari is exposed, primarily, to northerly winds with an average speed of 4.5 m/s and maximum speeds exceeding 21 m/s. These winds generate offshore-propagating waves with periods up to 9 s. The coastal zone of Koutsounari is affected mainly by wind-generated waves from SE, S and SW, with offshore significant wave heights up to 6 m and peak periods exceeding 10 s (Ghionis et al., 2014). The general orientation of the shoreline is E-W and the beach faces the Libyan Sea with a maximum fetch length of 508 km. The beach consists of sandy gravel or gravel, has a length of 567 m and a mean width of 50 m.

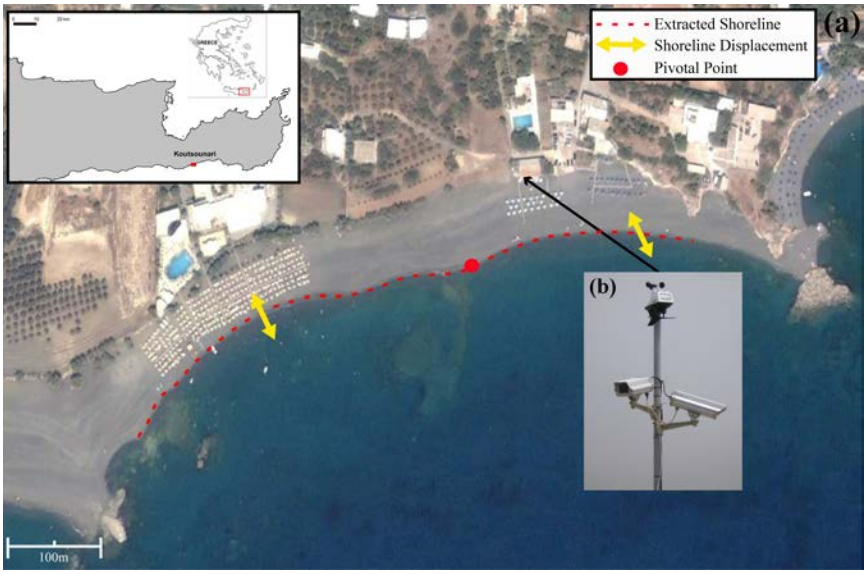

Fig.1. Satellite image of the study area showing the extracted shoreline, the beach displacements and the pivotal point (a), and the video monitoring system together with the weather station (b) (Image source: Google Earth).

3. Methodology

3.1 Coastal Monitoring

Two Point Grey Flea2, Firewire 800 video cameras with 1.2 MP resolution, were installed on a mast above the roof of the restaurant "Pelagos" in Koutsounari beach (Fig. 1). The elevation of the center of view (COV) was 14m above MSL. The cameras were connected to a PC and the system was set up to monitor a coastal stretch measuring 460m alongshore with image acquisition taking place at 4Hz, at hourly 10min bursts from 06:00am to 06:00pm. The monitoring period was from 26 November 2012 to 26 May 2013, with the exception of the periods 1-3/1/2013, 10-19/3 2013, 24/4 to 13/5/2013 and 16-19/5/2013, when the system was inoperative due to technical problems related to the electrical power supply.

Both cameras were calibrated in the field. The internal calibration included procedures for the determination of the intrinsic camera parameters, such as lens distortion, field of view and sensor response. The external calibration included the camera position and the angles of camera tilt, azimuth and roll. The method of transformation from real-world coordinates (X, Y, Z) to undistorted image coordinates (U, V) is described by Hartley and Zisserman (2003) and is based on ground control points (GCPs). In this study 20 GCPs were surveyed with RTK-DGPS for each camera and plan view images were generated with a horizontal resolution of 0.2 m, projected on a horizontal plane with elevation equal to the mean water level z_0.

The raw images were processed in situ to produce snapshot images, time-averaged (TIMEX) images, variance images (SIGMA) and timestack images (as defined by Holman and Stanley, 2007). The single snapshot image is usually collected at the beginning of each hour for each camera to record the conditions and provide a picture of the coastal zone. The timex image is computed hourly and represents the mathematical time-mean of all of the frames collected at 4Hz over a 10-minute period of sampling. Moving features such as waves are averaged out and only their mean brightness is returned (Fig. 2a). The sigma images are computed from the variance of image intensities of the same set of image samples. Areas that varied strongly in the raw images appear bright in the sigma images, e.g. the surf zone will appear very bright, due to the breaking waves (Fig. 2b).

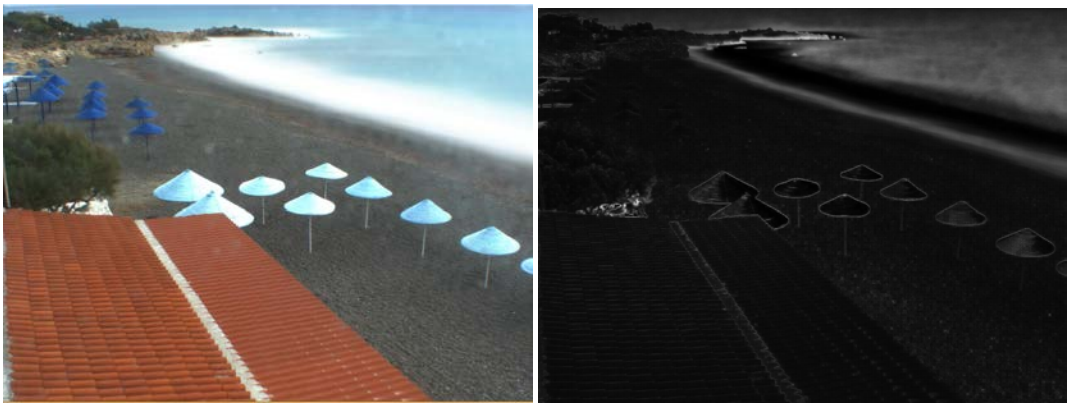

Fig. 2. TIMEX image (a) and SIGMA image (b) from the eastern camera (30 November 2012, 12:00)

The shoreline detection procedure was based on the sigma images (a total of 1363 images were used) with the use of a GUI shoreline extraction tool (Vousdoukas et al., 2011). The region of interest (ROI) was selected and the sigma images were georectified in a rotated metric coordinate system, such that the x and y directions represent longshore and cross-shore distance respectively. The shoreline was extracted automatically using an intensity threshold exceedance criterion and was corrected manually, when necessary.

3.2 Environmental (wave, tidal, topographic) measurements

The beach face was surveyed with RTK-DGPS, at the beginning and the end of the study period. Bathymetric data were collected with the use of RTK-DGPS up to a water depth of 1.5 m and with an echo-sounder between 1.5 and 40 m water depth. A Starfish side scan sonar was used to map the seafloor.

The variations of sea surface elevation were recorded every 10min, from 26 October 2012 to 23 May 2013, by a HOBO U20-001-01 water level recorder, that was installed 30 cm above the seafloor at 10.5 m water depth. The data were corrected for barometric pressure variations and were used for the study of tidal sea level variations, wind set-up and set-down and storm surges.

A Davis Vantage Vue weather station was installed on October 28, 2012, on top of the mast that hosted the coastal imaging cameras. The weather station was wirelessly connected to the field computer and recorded the wind speed and direction, air temperature, relative humidity and barometric pressure, from 28/10/2012 to 01/10/2013, at 1 min intervals. The recorded wind speed was converted to wind stress factor and was used to hindcast the deep-water wave characteristics for each storm, according to CERC (1984).

The wave run-up for each storm was estimated using the Stockdon et al. (2006) formulation:

$$R_2 = 1.1\left(0.35 \cdot \beta_f \cdot (H_0 \cdot L_0)^{1/2} + \frac{\left[H_0 \cdot L_0 \cdot \left(0.563 \cdot \beta_f^2 + 0.004\right)\right]^{1/2}}{2}\right)$$

where H_0, L_0 are the wave height and wavelength in deep water respectively and β_f is the foreshore slope (=0.24), as surveyed on 20 August 2012.

4. Results-Discussion

Ten storms from southerly directions were recorded during the monitoring period (26 November 2012 to 26 May 2013) (Fig. 3). The highest waves (H_0=0.96m) and the highest wave run-up (R_2=1.0 m) occurred during the storm of 7-8 February 2013, which had 12 hours duration and SSW prevailing winds.

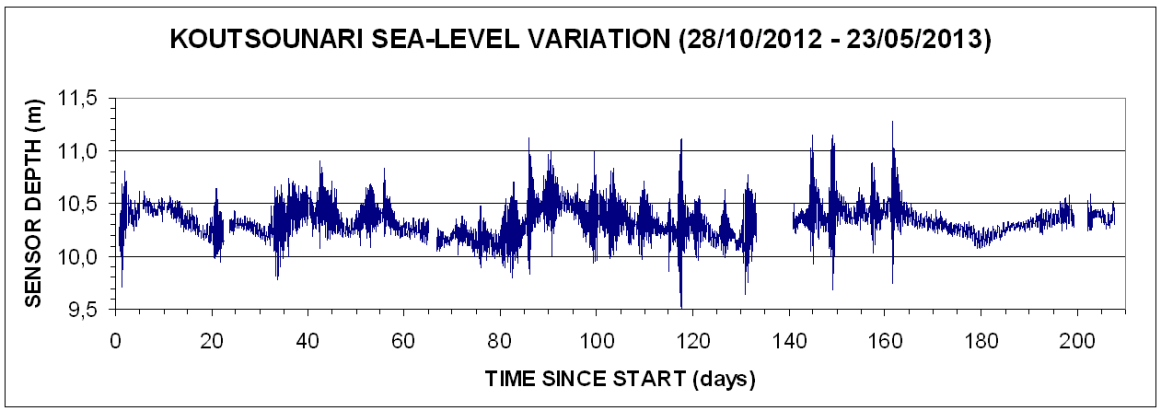

Fig. 3 Time series of sea surface elevation recorded at Koutsounari beach from 28/10/2012 to 23/5/2013

The extracted shoreline positions of the entire region of interest (ROI) during the study period are presented in Figure 4. The maximum shoreline displacement (maximum shoreline advance – maximum shoreline retreat) of the middle section of the study beach is 40 m, while at the western and eastern ends of the beach the maximum shoreline displacements are 60m and 20m, respectively.

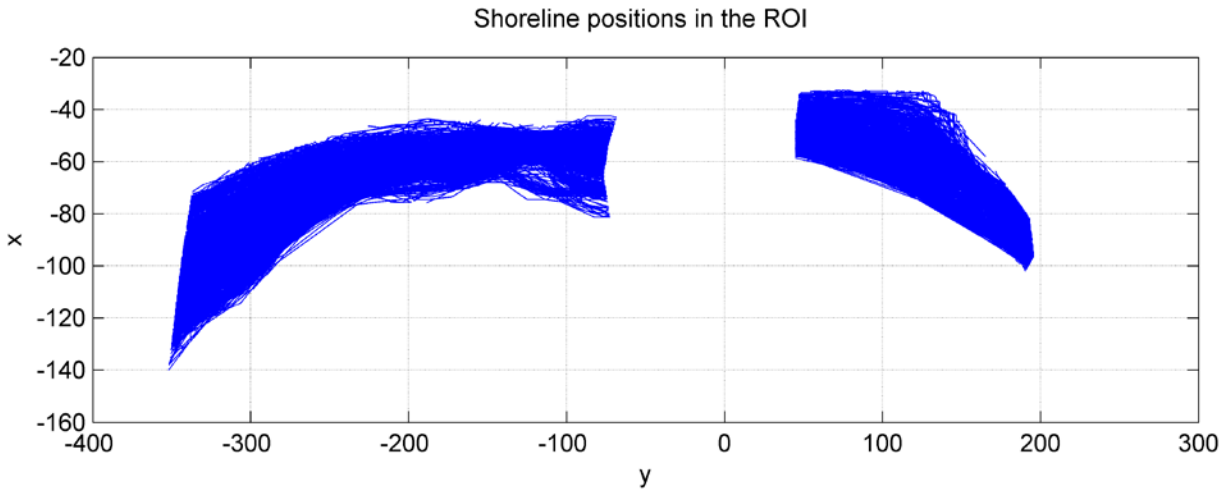

Fig. 4 The extracted shoreline positions for the period 26/11/2012-26/5/2013 in image coordinates.

(0,0) is the camera position, X is the cross-shore distance, y is the longshore distance.

Figures 5a and 6a show the measured camera-shoreline horizontal distances in the region of interest during the monitoring period. A prominent feature is the periodicity of shoreline displacement, which is linked directly to the tidal oscillations in the nearshore zone.

Figures 5b and 6b show one-day and three-day average shoreline distances, respectively, for the whole region of interest during the monitoring period, and Figures 5c and 6c show the corresponding shoreline changes.

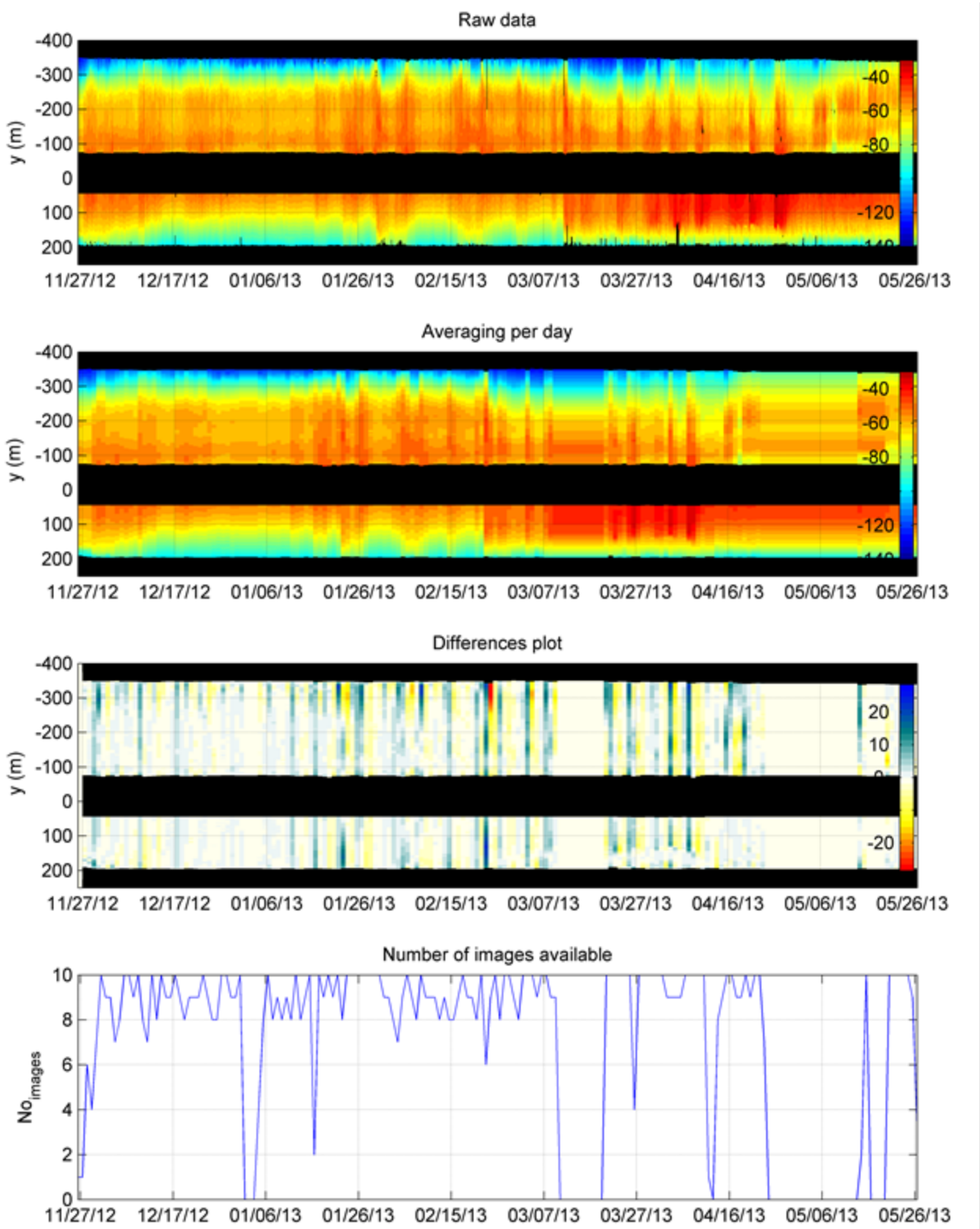

Fig. 5 Extracted shoreline positions (a), Daily-averaged shoreline positions (b), Daily differences in shoreline position (c) and Number of images used for the computation of the average values (d). In the Differences plot, the blue colour indicates accretion and the red indicates erosion.

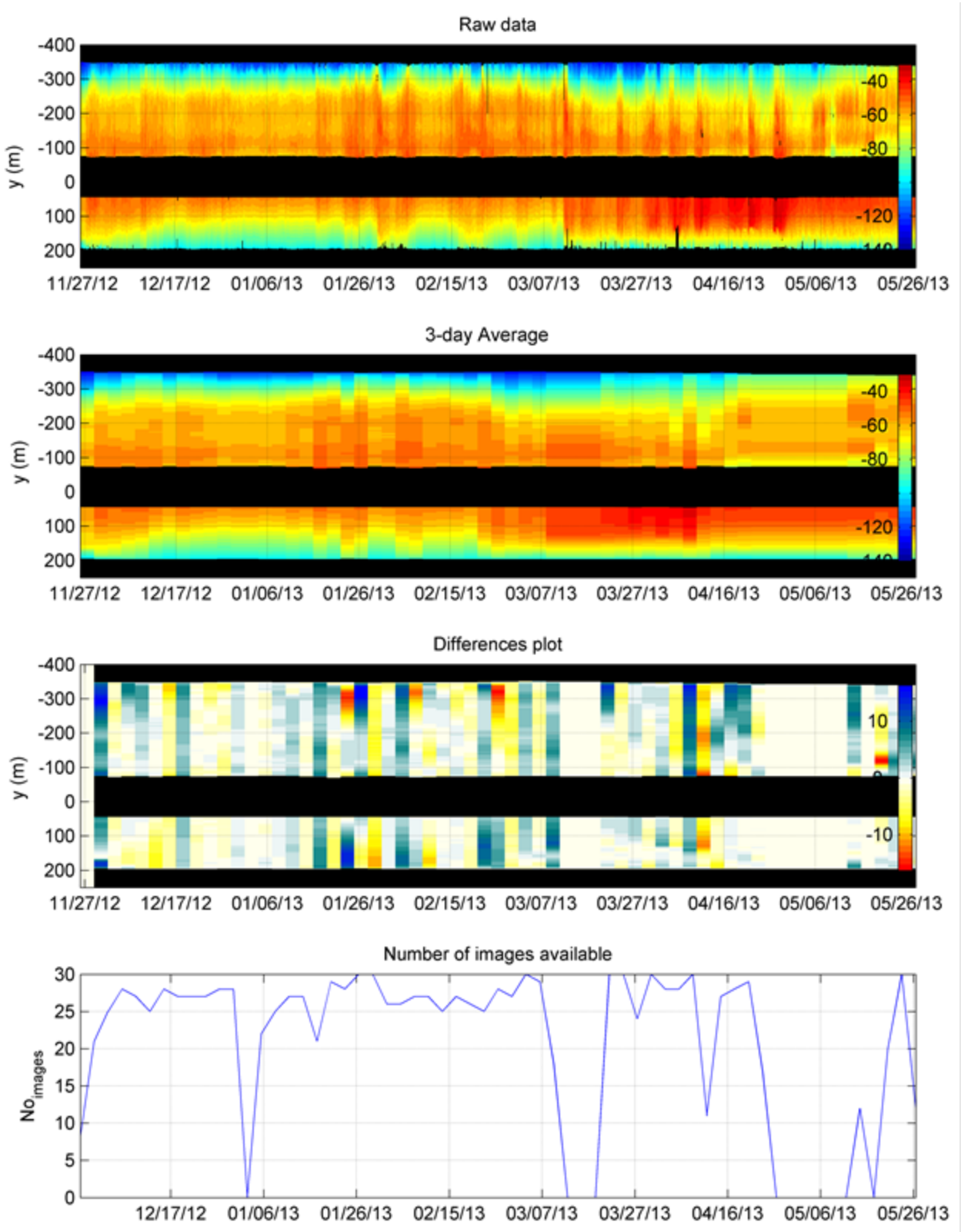

Fig. 6 Extracted shoreline positions (a), 3-day average shoreline positions (b), 3-day differences in shoreline position (c) and Number of images used for the computation of the average values (d). In the Differences plot, the blue colour indicates accretion and the red indicates erosion.

The video results were also compared to the estimated wave run-up and the significant wave height H_s for each storm. The maximum wave run-up was recorded during the fourth and ninth storms (0.81 m and 1.0 m, respectively), when the prevailing winds were from SSW and accretional events occurred.

Furthermore, from the predicted wave data (direction and significant wave height) of the TRITON wave forecasting system, which are presented in Figure 7a,b, it seems that the shoreline retreat is better correlated to the significant wave height than to the wave direction, with the erosion events been recorded during theH_s maxima, while the wave direction seems to be ESE-SSE for all of monitoring period.

Figure 7c,d shows that most of the storms caused erosion except for the fourth, ninth and tenth where both of parts of the beach advanced. The maximum erosion occurred during the storms of 27 January 2013 and 5-9 April 2013, when the prevailing winds were from SSW. Additionally, it must be noted that the erosional events were followed by recovery of similar magnitude (Fig.7d). The same pattern was observed during the 19 December, 16 January, 27 January, 1 March and 8 April erosional events, which were followed by rapid recovery (within 24h).

The behavior of both parts of the beach is for the most of the monitoring period synchronous, which means that they respond in unison to changing wave height (Fig. 7d). However, four events of beach rotation were noticed during the study period (on 5-12 December 2012, 21-25 January 2013, 4-7 February 2013, and 24-29 February 2013). The pivotal point is generally located in the central region of the beach, as depicted in Figure 1a. These rotation events are associated to an alongshore sediment transport from the updrift to the downdrift end of the beach, generating erosion in the first part and accretion in the other (Turki et al., 2013). During the first and third rotation events the western shoreline advanced and the eastern retreated, while during the second and fourth rotation events the western shoreline retreated and the eastern advanced, as illustrated in Figure 6d. The first rotation event occurred during the second storm, when SE winds prevailed, and the second rotation event occurred during the fifth storm, when SSW winds prevailed. The successive shoreline positions and displacements during the study period are presented in Figure 7c,d, with maximum shoreline advance and retreat both exceeding 9 m.

Most of the sediment transport in the study area is in the on-offshore direction, as both parts of the beach retreat or advance simultaneously for most of the monitoring period, while the longshore sediment transport occurs mainly during the pivoting periods of the Koutsounari beach.

The shoreline retreat appears to be controlled by the significant wave height as far as the eastern part of the beach is concerned. Figure 8 depicts the high correlation between the significant wave height and the shoreline retreat of the eastern part of the beach (R^2=0.79). However, the same calculations for the western part of the beach did not have similar results and the correlation was significantly lower.

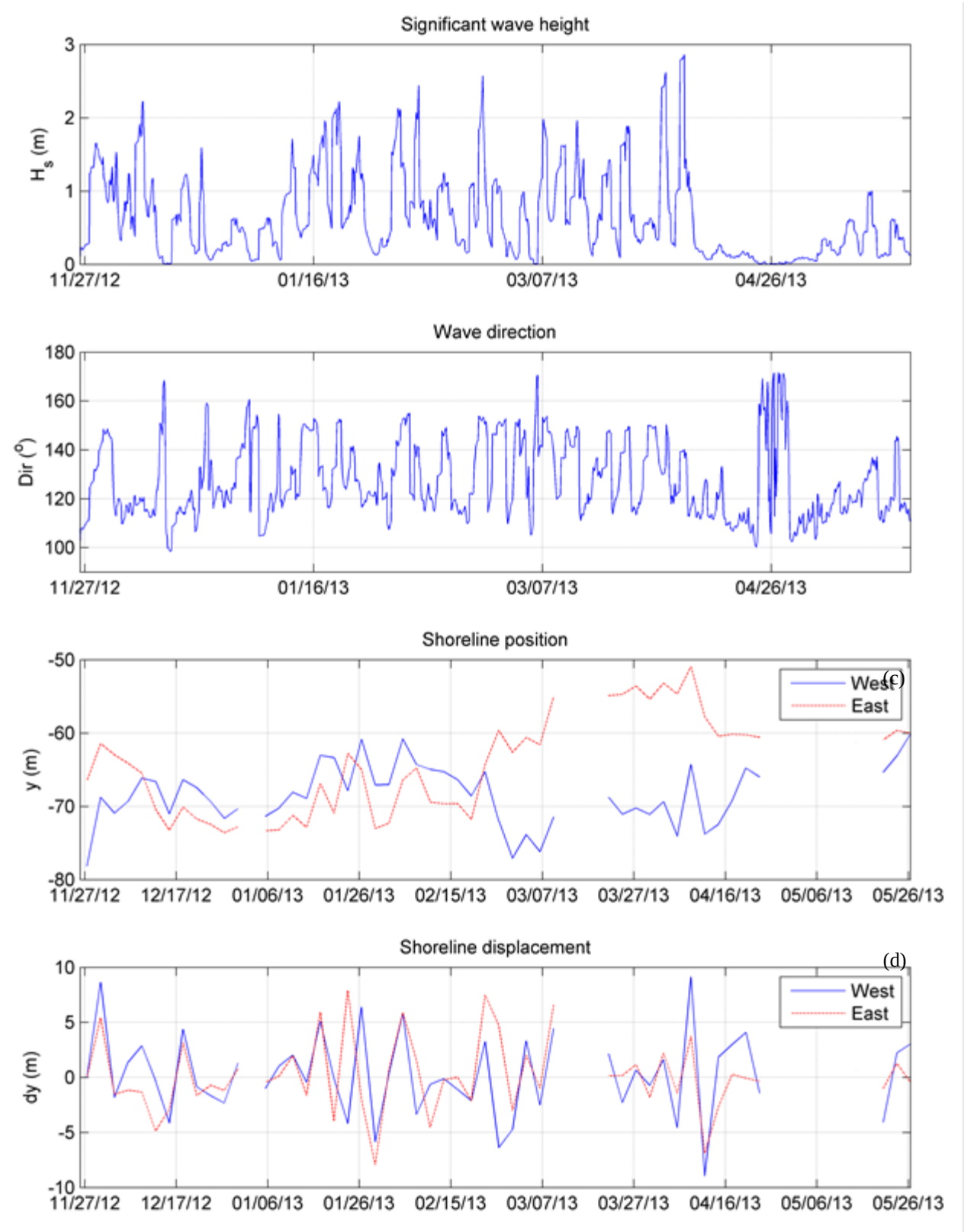

Fig. 7 Significant wave height (a), wave direction (b), shoreline position (c), and shoreline displacement (d)

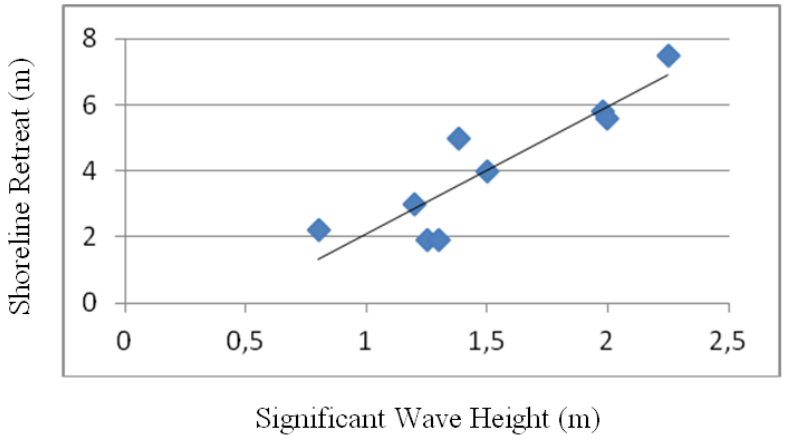

Fig. 8 Correlation between shoreline retreat and significant wave height H_s

A related study by Monioudi et al. (2013), based on numerical modeling, showed that in the case of a sea level rise of 0.86 m the beach will retreat 9.6 m (which is in agreement with the observations during the present study) while in the case of a sea level rise of 1.86 m the beach will retreat 21.5m.

Conclusions

The video-based coastal imaging system, combined with advanced processing and analysis software tools, proved to be an invaluable tool for the detailed study of beach response to changing hydrodynamic conditions. The high rate of image acquisition allowed the extraction of successive shoreline positions with sufficient spatial and temporal resolution, so that shoreline changes could be correlated to the observed meteorological and hydrodynamic conditions in the Koutsounari coastal zone. Most of the time, the whole length of the shoreline responds in unison (either advancing or retreating) to changes in hydrodynamic conditions and sediment transport is in the on-offshore direction. During storms the shoreline retreats, as erosional processes prevail, but recovery is rapid (within 24 h) after the storms. Significant longshore transport rates are associated with ESE-SSE and SSW incoming waves and are manifested as beach rotation events. The highest recorded wave run-up was 1.0 m. The eastern part of the beach is more vulnerable to the prevailing wave direction (ESE-SSE) and increased significant wave heights than the western part.

Acknowledgements

The authors would like to thank Dr. S. Sofianos for sharing the wave data of the TRITON wave forecasting system. This study was carried out within the framework of the project “Cooperation 2007-2013” (09SYN-31-711 “AKTAIA”) of the Operational Program “Competitiveness and Entrepreneurship”, which is co-funded by the European Regional Development Fund (ERDF) and the General Secretariat for Research and Technology (Hellenic Ministry of Education).

References

Aarninkhof, S.G.J., Turner, I.L., Dronkers, T.D.T., Caljouw, M., Nipius, L., 2003. A video-based technique for mapping intertidal beach bathymetry. Coast Eng 49:275-289.

Archetti R., Schiaffino C.F., Ferrari M., Brignone M., Rihouey D., 2008. Video systems for coastal monitoring. Beach Erosion monitoring. Results from BEACHMED-e/OpTIMAL Project.

Carter, R.W.G., 1988. Coastal Environments. An introduction to the Physical, Ecological and Cultural Systems of Coastlines. Academic Press Limited. London.

C.E.R.C., 1984. Shore Protection Manual (Fourth edition). Coastal Engineering Research Center, U.S. Army Engineer Waterways Experiment Station, Vicksburg, Miss.

Crowell, M., Leatherman S.P., Buckley M.K., 1991. Historical Shoreline Change: Error Analysis and Mapping Accuracy. J Coast Res, 7 (3), 839-852.

EUSORION, 2001. Coastal erosion- Evaluation of the need for action. Directorate General Environment, European Commission.

Ghionis, G., Alexandrakis, G., Karditsa, A., Sifnioti, D., Vousdoukas, M., Andreadis O., Petrakis, S., Poulos, S., Velegrakis, A., Kampanis, N., Lipakis, M., 2014. An integrated multi-parameter monitoring approach for the quantification and mitigation of the climate change impact on the coasts of Eastern Crete, S. Aegean Sea (Project AKTAIA). Geophysical Research Abstracts Vol.16, EGU2014-11685, EGU General Assembly 2014.

Hartley, R., Zisserman, A., 2003. Multiple view geometry in computer vision. Cambridge University Press. Second Press.

Holman, R.A., Stanley, J., 2007. The history and technical capabilities of Argus. Coastal Engineering, 54, 477-491.

Monioudi I.N., Karditsa A., Alexandrakis G., Poulos S.E., Velegrakis A.F., Andreadis O.P., Ghionis G., Petrakis S., Sifnioti D., Markakis E., Giannouli D.I., 2013. Vulnerability Assessment of Eastern Cretan Beaches (Greece) to sea level rise. ADAPTtoCLIMATE Conference electronic proceedings, 27-28 March 2014, Nicosia Cyprus.

Plant, N.G., Holman, R.A., 1997. Intertidal beach profile estimation using video images. Mar Geol 140(1-2):1-24

Plant N.G., Aarninkhof S.G.J., Turner I.L., Kingston K.S., 2007. The Performance of Shoreline Detection Models applied to Video Imagery. J Coast Res, 23(3), 658-670.

Stockdon, H.F., Holman, R.A., Howd, P.A., Sallenger, A.H., 2006. Empirical parameterization of setup, swash, and runup. Coastal Engineering, 53, 573-588.

Turki I., Medina R., Coco G., Gonzalez M., 2013. An equilibrium model to predict shoreline rotation of pocket beaches. Mar Geol, 346, 220-232.

Vousdoukas, M.I., Velegrakis, A.F., Dimou, K., Zervakis, V., Conley, D.C., 2009. Wave run-up observations in microtidal, sediment-starved pocket beaches of the Eastern Mediterranean. J Mar Syst 78:37-47.

Vousdoukas, M.I., Ferreira, P.M., Almeida, L.P., Dodet, G., Andriolo, U., Psaros, F., Taborda, R., Silva, A.N., Ruano, A.E., Ferreira, O., 2011. Performance of intertidal topography video monitoring of a meso-tidal reflective beach in South Portugal. Ocean Dynamics, 61, 1521-1540.

Vousdoukas, M.I., Wziatek, D., Almeida, L.P., 2012. Coastal vulnerability assessment based on video wave run-up observations at a mesotidal, steep-sloped beach. Oc Dyn 62:123-137.

Vousdoukas, M.I., 2012. Erosion/accretion patterns and multiple beach cup systems on a meso-tidal, steeply-sloping beach. Geomorphology, 141-142, 34-36.